Static and dynamic properties of water-in-oil microemulsions near the critical and percolation points

1994 J. Phys.: Condens. Matter 6 10855

(http://iopscience.iop.org/0953-8984/6/50/002)

J. Phys.: Condens. Matter 6 (1994) 10855–10883. Printed in the UK

REVIEW ARTICLE

Static and dynamic properties of water-in-oil microemulsions near the critical and percolation points

S H Chen†, J Rouch‡, F Sciortino§ and P Tartaglia§

† Department of Nuclear Engineering and Center for Material Science and Engineering, Massachusetts Institute of Technology, Cambridge, MA 02139, USA

‡ Centre de Physique Moléculaire Optique et Hertzienne (URA 283 du CNRS), Université Bordeaux I, 351 Cours de la Libération, 3405 Talence, France

§ Dipartimento di Fisica, Università di Roma La Sapienza, Piazzale Aldo Moro 2, I-00185, Roma, Italy

Received 12 August 1994

Abstract. The three-component ionic microemulsion system consisting of AOT/water/decane shows an unusual phase behaviour in the vicinity of room temperature. The phase diagram in the temperature–volume-fraction (of the dispersed phase) plane exhibits a lower consolute critical point at about 40 °C and 10% volume fraction. A percolation line, starting from the vicinity of the critical point, cuts across the plane, extending to the high-volume-fraction side at progressively lower temperatures. This phase behaviour can be understood in terms of a system of polydispersed spherical water droplets, each coated by a monolayer of AOT, dispersed in a continuum of oil. These droplets interact with each other via a hard-core plus a short-range attractive interaction, the strength of which increases with temperature. We show that Baxter's sticky-sphere model can account for the phase behaviour, including the percolation line, quantitatively provided that the stickiness parameter is a suitable function of temperature. We use the structure factors measured by small-angle neutron scattering (SANS) below the critical temperature to determine this functional dependence. We also investigate the dynamics of droplets, below and approaching the critical and percolation points, by dynamic light scattering. The first cumulant and time evolution of the droplet density correlation function can be quantitatively calculated by assuming the existence of polydispersed fractal clusters formed by the microemulsion droplets due to attraction. The relaxation phenomena observed in an extensive set of measurements of electrical conductivity and permittivity close to percolation can also be interpreted through the same cluster-forming mechanism, which reproduces the most relevant features of the frequency-dependent complex dielectric constant of this system.

1. Introduction

Three-component microemulsion systems made of ionic or non-ionic surfactants, water and oil exhibit interesting phase behaviour in the vicinity of room temperature. At a characteristic temperature where the surfactant has balanced affinities toward water and oil, called the hydrophile–lipophile balance (HLB) temperature, a typical symmetric ternary microemulsion system, having equal volume fractions of water and oil, shows the well known 2–3–1 phase progression, as the surfactant concentration is increased from zero to more than 8% [1]. When surfactant concentration is very low, the molecules are dispersed in water and oil as monomers. The system is naturally separated into two phases, with an oil-rich phase on the top (lighter) and water-rich phase on the bottom (heavier) because of high interfacial tension between water and oil. There is no discernible organized microstructure in the two phases. At relatively higher surfactant concentrations, a three-phase coexistence,

0953-8984/94/5010855+29$19.50

with a middle-phase microemulsion in coexistence with an oil-rich phase on the top and a water-rich phase on the bottom, is to be expected simply because of a finite and equal solubilization power of the surfactant for water and oil. The middle-phase microemulsion is an interesting liquid because there is an organized microstructure in it [2]. The microemulsion shows ultralow interfacial tensions between itself and the water and oil-rich phases. The micro-structure of the middle-phase microemulsion is often described as being *bicontinuous* in both water and oil [3]. With further increase in the surfactant concentration, a *minimum* concentration will be reached whereby all the excess water and oil are solubilized into a single-phase microemulsion. This *minimum* concentration is usually between 5 and 8% for a *good* microemulsion system. The value of the minimum concentration is a measure of the amphiphilicity of the surfactant molecules at that temperature, being lower for higher amphiphilicity. In the vicinity of this minimum surfactant concentration, the microstructure of the one-phase microemulsion is disordered bicontinuous [4]. As the surfactant concentration further increases, the one-phase microemulsion transforms into a lamellar structure, which may be called an ordered bicontinuous structure, and then to some other three-dimensional ordered structures. This disorder-to-order transition occurs usually around 15% of the surfactant concentration [4]. Away from the HLB temperature, the phase progression as a function of surfactant concentration is different because at these temperatures the surfactant film, located in between water and oil, aquires a spontaneous curvature. Depending on the sign of the curvature, a two-phase coexistence, with either a water-in-oil (W/O) microemulsion on the top and a water-rich phase on the bottom or with an oil-in-water (O/W) microemulsion on the bottom and an oil-rich phase on the top, becomes possible for moderate concentrations of the surfactant. Micro-structures of W/O or O/W microemulsions are likely to be a droplet type. The AOT/water/decane system does not follow, however, this usual pattern of phase behaviour. Around room temperature, or more specifically from 10 to 50 °C the surfactant film, consisting of AOT molecules having a bulky tail and a small head, possesses a spontaneous curvature toward water due to the hydrophilicity–lipophilicity imbalance of the AOT molecules. Thus, at room temperature, one finds in the ternary phase triangle a large one-phase region, called L2 phase, extending from the decane corner into the middle of the phase triangle. In the L2 phase, even with equal volume fractions of water and oil, the microemulsion, instead of being bicontinuous like other three-component microemulsion systems made of non-ionic (C_iE_j-type) surfactants, consists of water droplets, coated by a monolayer of AOT, dispersed in decane [5]. With this microstructure, the microemulsion is basically an insulator, having a conductivity of the order of $10^{-6}\ \Omega^{-1}\ m^{-1}$, because the water droplets are separated from each other. Our previous SANS experiments verified that the average radius $\langle R \rangle$ of the water droplets is determined essentially by the molar ratio of water to AOT, called W, in the system. An approximate empirical relationship between the radius (in Å) and W is $\langle R \rangle = \frac{3}{2}W$. Thus, for $W = 40$, the average water-droplet radius is about 60 Å [6]. This water-in-oil droplet structure is maintained even if the volume fractions of water and oil are equal [5], provided the temperature is below 25 °C. This case is in sharp contrast to the common situation that, for equal water and oil volume fractions, the microstructure of one-phase microemulsions were generally found to be bicontinuous [7, 8]. Even for the AOT/water/decane system, when a small amount of salt (NaCl) is added, the common 2–3–1 phase progression is obtained at around the hydrophile–lipophile balance temperature of 40 °C [4] and a SANS experiment in the one-phase channel around this temperature conclusively showed that the microstructure is bicontinuous [4, 9]. This persistent droplet structure in the ternary AOT/water/decane system can, however, be used to realize an interesting coexistence of a critical phenomenon at low volume fraction and high temperature and a percolation phenomenon at lower temperatures

but at all volume fractions. In fact, this is a rare situation in which one can study, in a real system, the analogy, both in the static and dynamic properties, between approaching the critical point and percolation point in temperature from below at the same volume fraction. We shall stress this analogy throughout this paper. Figure 1 shows the $(T-\phi)$ phase diagram of the AOT/H_2O/decane system when the water-to-AOT molar ratio is $W = 40.8$. Substitution of H_2O by D_2O merely shifts all the phase boundaries up by about 2 °C. ϕ denotes the volume fraction of the dispersed phase, in this case the AOT plus water. In the $(T-\phi)$ diagram, one sees a one-phase (L2) region below 40 °C. In the interval of ϕ between zero and 0.4, there is a cloud-point curve separating the one-phase droplet microemulsions from two-phase droplet microemulsions. The previous SANS experiment established that the average droplet sizes and their size distributions are, within the experimental error, identical in the one-phase and two-phase regions [6]. The critical volume fraction is approximately 0.1 and the critical temperature is 40 °C [10] in H_2O-based microemulsions. Above the volume fraction of 0.4 there is a phase boundary between the L2 and a lamellar phase where the microstructure is ordered and bicontinuous in water and decane. The novelty of this phase diagram is, however, the existence of a percolation line, extending from the left of the critical point, all the way to higher volume fractions, gradually decreasing in temperature to about 23 °C at $\phi = 0.7$. Below the percolation line the microemulsion is non-conducting but above the percolation line it becomes conducting. In crossing the line, the conductivity increases by over five orders of magnitude. Figure 2 shows a set of DC conductivities σ (plotted in a logarithmic scale) as functions of T and ϕ [11]. One sees clearly a set of steeply rising sigmoidal curves that can be used to define a set of loci (T_p, ϕ_p) in terms of their inflection points. The asymptotic behaviour of the DC conductivity near the threshold, at a given ϕ, can be expressed as

$$\sigma = A\left(\frac{T_p - T}{T_p}\right)^{-s'} \tag{1}$$

coming up from below, and

$$\sigma = B\left(\frac{T - T_p}{T_p}\right)^{t} \tag{2}$$

going down in temperature from above. The exponents s' and t have been determined experimentally to be 1.2 ± 0.1 and 1.9 ± 0.1 respectively [11]. These exponents are the same when T is fixed but ϕ is varied [11]. The exponent s', determined from conductivities below the threshold, agrees with the value of the index proposed in the so called dynamic percolation theory [12, 13], which is distinct from the standard static percolation exponent $s = 0.73$ [14]. On the other hand, the exponent t deduced from data above the threshold agrees with the static or geometric percolation theory [14]. In the theory of dynamic percolation, the conduction of electricity is conjectured to be mediated by charge carriers (presumably the sodium counterions from the AOT molecules) which migrate rapidly among microemulsion droplets forming transient fractal clusters, due to a short-range attractive interaction between the droplets. The percolation threshold is defined theoretically to be the point where the average cluster size becomes infinity, namely, when at least one cluster spans the entire sample. Figure 3 depicts the asymptotic behaviour of the DC conductivity by plotting scaled conductivities $T_p(\sigma/A)^{1/s'}$ and $T_p(\sigma/B)^{-1/t}$ as a function of $T - T_p$, for several volume fractions. It is seen that above the threshold, all the data at different volume fractions follow the asymptotic relation (2) very well. However, below the threshold, the

asymptotic relation (1) holds better for higher volume fractions. For lower volume fractions, say below $\phi = 0.4$, the range of validity ΔT is very small. Thus experimentally the manifestation of dynamic percolation is observable only when ϕ is greater than about 0.45. We have thus experimental evidence that the electrical percolation in the AOT/water/decane system in the L2 phase is associated with a clustering phenomenon. The phase diagram that we depicted in figure 1 should therefore be obtainable from the standard liquid theory with an appropriate definition of the percolation. We shall outline one such theory in the next section.

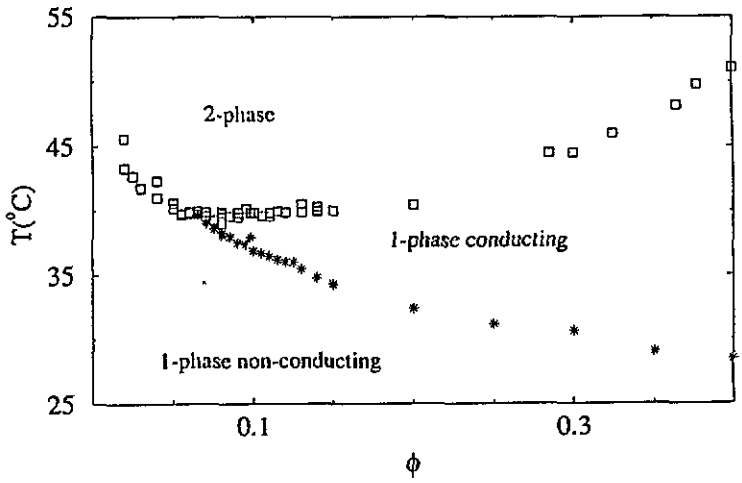

Figure 1. Projection of the phase prism of the AOT/H_2O/decane system, at $W = 40.8$ and at atmospheric pressure, on the temperature–volume-fraction plane. The open squares are the one-phase–two-phase boundary and the stars are percolation loci [11].

2. Baxter's sticky-sphere model and the associated phase diagram

A reasonable model for a microemulsion in the L2 phase is to regard it as a collection of spherical colloidal particles of average radius $\langle R \rangle$ interacting among one another via a short-range temperature-dependent attractive pair potential (or more appropriately a potential of the mean force). This pair potential can, for example, be a square-well potential with a hard-core diameter $a - \Delta$, plus an attractive well of depth $-\epsilon$ and width Δ. In order to show a pictorial representation of the clustering process we have performed a numerical simulation of the square-well potential, $a = 1.02$, $\Delta = 0.02$ (in units of the inner diameter of the attractive well σ), and $\beta\epsilon \approx 3.7$, where $\beta = 1/k_B T$. Figure 4(*a*) shows the growth of the largest fractal cluster of connected nearest-neighbour droplets as a function of the volume fraction of the dispersed phase from 0.05 to 0.45, the percolation threshold for the parameters we used can be located between the second and the third figure of the sequence. Similar figures are obtained as a function of temperature. Figure 4(*b*) shows nearest-neighbour clusters, at $\tau = 0.1$ and $\phi = 0.1$.

The liquid theory with an arbitrary square-well potential cannot be solved in an analytical form, except for a limiting case in which ϵ tends to infinity and Δ to zero in such a way that a contribution of the attractive tail to the second virial coefficient exists. This limiting

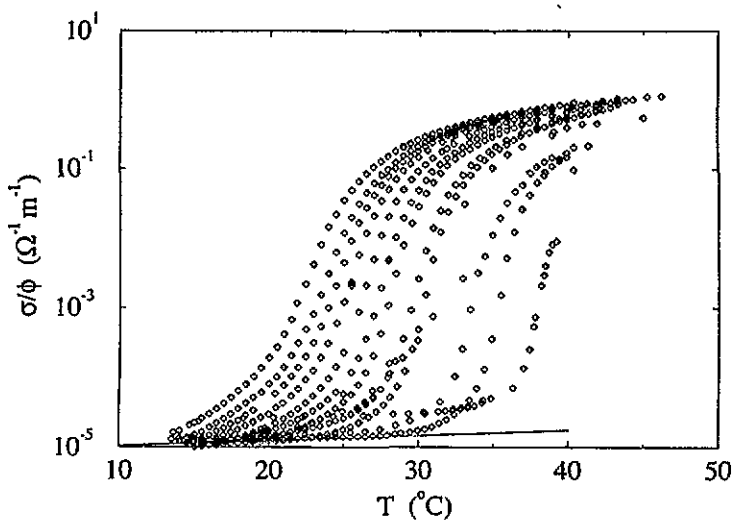

Figure 2. DC electrical conductivity divided by the volume fraction of the AOT/H_2O/decane system as a function of temperature for different volume fractions (from 9.8%, right, to 65%, left) and showing the percolation behaviour [11]. Note that the percolation temperature starts at about 40 °C at 9.8% and progressively decreases to about 22 °C at a volume fraction of 65%.

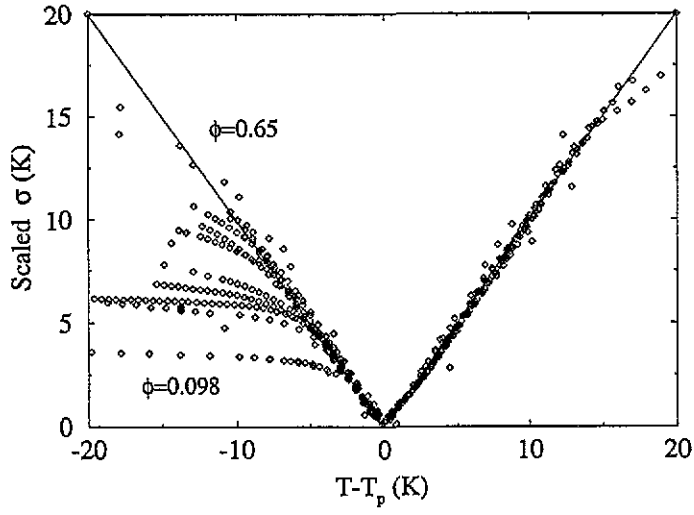

Figure 3. The scaled conductivities $T_p(\sigma/A)^{1/s'}$ and $T_p(\sigma/B)^{-1/t}$ are plotted as a function of $T - T_p$ at different volume fractions, showing the power-law behaviour near T_p [11]. Note that at low volume fractions percolation behaviour approaching from below is not well defined.

potential is called Baxter's sticky-sphere potential. Specifically, the pair potential is of the form

$$\beta u(r) = \begin{cases} +\infty & r < \sigma \\ -\ln\left[\dfrac{a}{12\tau\,(a-\sigma)}\right] & \sigma < r < a \\ 0 & r > a. \end{cases} \tag{3}$$

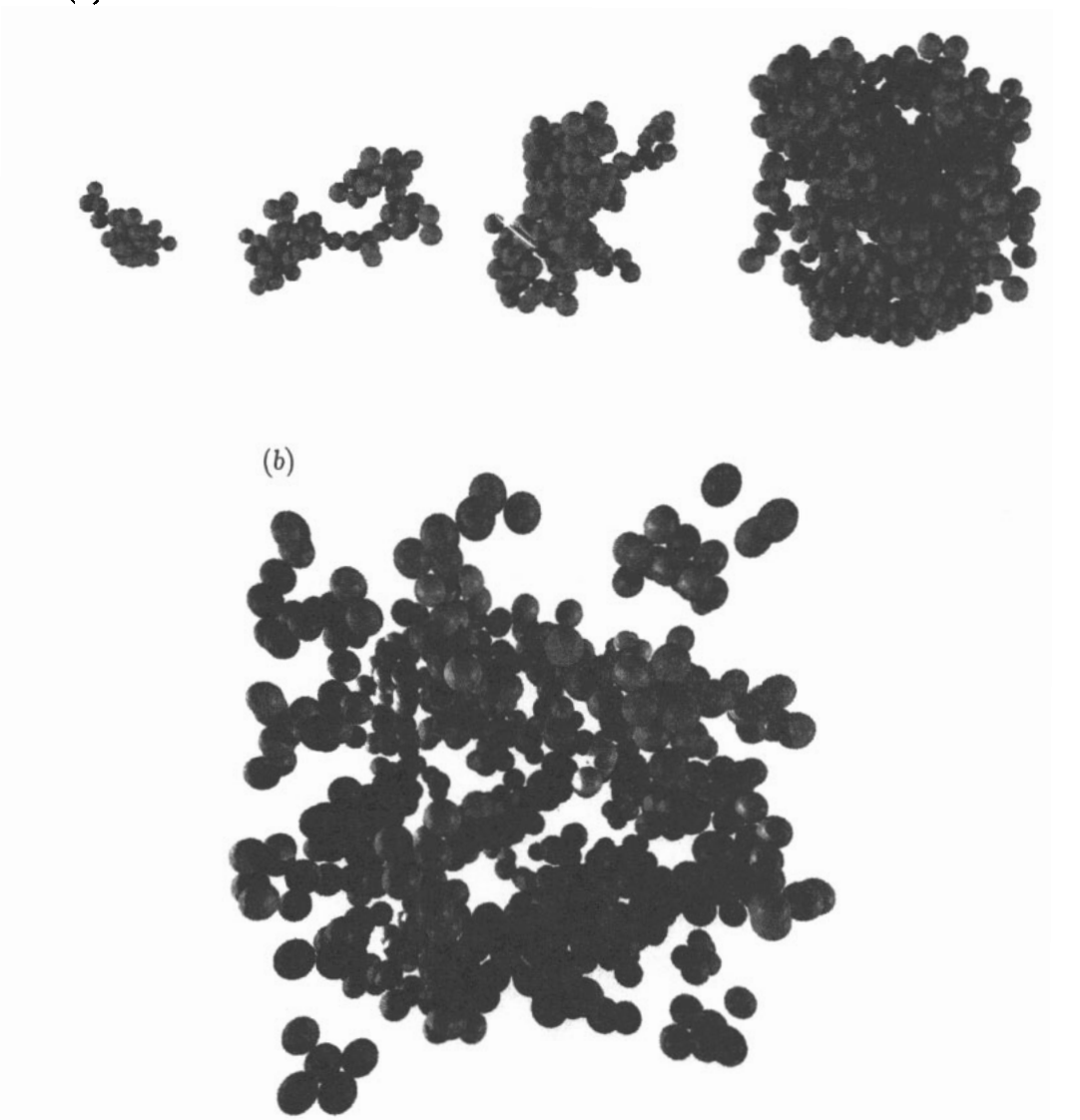

Figure 4. (*a*) The growth of the largest fractal cluster of connected nearest-neighbour droplets as a function of the volume fraction of the dispersed phase from 0.05 to 0.45. Snapshots taken from a Monte Carlo numerical simulation of the square-well potential with parameters $a = 1.02$, $\Delta = 0.02$, and $\beta\epsilon = 3.7$, equivalent to Baxter's model with $\tau = 0.1$. (*b*) A snapshot of the system, showing differently shaded nearest-neighbour clusters, at $\tau = 0.1$ and volume fraction of the dispersed phase 0.1.

It is understood that the limit $\sigma \to a$ is to be taken in the calculation. From our discussion above, it is obvious that the magnitude of $a - \Delta$ is about $2\langle R \rangle$. The dimensionless parameter $1/\tau$ is called the stickiness parameter. The sphere is stickier the smaller the value of τ is. In the limit of τ tending to infinity, the pair potential reduces to a hard-sphere potential. Assuming $a \ll \Delta$ and using a perturbation theoretical solution for the square-well potential

to the lowest order in Δ/a, one gets a relation [15]

$$\frac{1}{\tau} = \frac{12\Delta}{a} \exp(\beta\epsilon). \tag{4}$$

It is seen from (4) that the stickiness increases as Δ/a or $\beta\epsilon$ increase. For AOT molecules in decane, the parameter Δ should correspond roughly to the length of the hydrocarbon tail. The tail could take an increasingly stretched conformation as temperature increases, thus increasing the interaction strength among droplets.

Baxter showed [16] that the Ornstein–Zernike equation using this sticky pair potential can be solved analytically in the Percus–Yevick (PY) approximation. The PY approximation amounts to the reasonable *ansatz* that the direct correlation function $c(r) = 0$ outside the range of the potential a. Combining this *ansatz* with the exact boundary condition for hard spheres and knowing that the pair-correlation function $g(r) = 0$ inside the hard core, the direct correlation function inside the hard core can be found to be a polynomial of r. Thus one can obtain an analytical form of the three-dimensional Fourier transform of the direct correlation function $c(k)$ as a function of the volume fraction of the spheres η and the stickiness parameter $1/\tau$. Here, $\eta = \rho a^3\pi/6$, and ρ is the number density of the spheres. In comparing the theory with experiments for the scattering intensities, we shall identify η with ϕ.

First, the interparticle structure factor $S(k)$ is calculated from the relation

$$S(k) = \frac{1}{1 - \rho c(k)}. \tag{5}$$

From the limiting value $S(k \to 0) = \rho k_B T \chi_T$ we get the isothermal compressibility χ_T. By integrating χ_T with respect to the number density, one obtains the compressibility equation of state

$$\frac{\beta p}{\rho} = \frac{1 + \eta + \eta^2}{(1-\eta)^3} - \frac{\lambda\eta(1-\eta)(1+\eta/2) - \frac{1}{36}\lambda^3\eta^2(1-\eta)^3}{(1-\eta)^3} \tag{6}$$

where the parameter λ, a function of η and τ, is given by the smaller real root of

$$\frac{\eta}{12}\lambda^2 - \left(\tau + \frac{\eta}{1+\eta}\right)\lambda + \frac{1+\eta/2}{(1-\eta)^2} = 0. \tag{7}$$

From the compressibility equation of state, one finds the existence of a gas–liquid phase transition with a critical point occurring at $\eta_c = 0.1213$ and $\tau_c = 0.0976$. Although different results are obtained using the energy route to the equation of state, computer simulations [17] do suggest that the compressibility results are probably the most accurate PY estimates of the position of the critical point. Again, by integrating the compressibility equation of state, Barboy [18] was able to obtain an analytical chemical potential μ valid both in the one- and two-phase regions. Having the chemical potential and pressure, one can then obtain the coexistence curve by solving for the coexisting gas and liquid densities at a given τ, which is less than τ_c in the two-phase region. Since in the AOT-based microemulsion system the stickiness between droplets increases as temperature increases, it is natural to plot the stickiness as a function of the volume fraction. Figure 5 shows such an inverted coexistence line obtained by plotting τ_c/τ against η/η_c. In the same figure the corresponding spinodal line is also plotted as a dashed line. The spinodal line is the locus of (τ, η) where

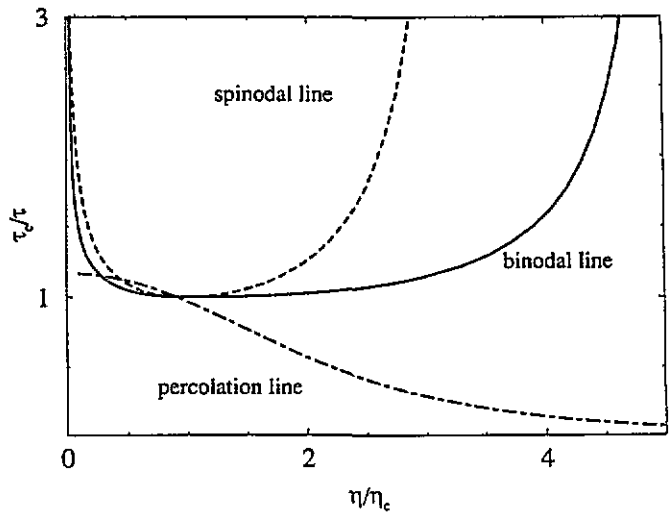

Figure 5. Theoretical percolation, coexistence and spinodal lines according to Baxter's model This figure gives locations of one- and two-phase, percolated and non-percolated regions in a plane defined by τ_c/τ and η/η_c according to the model.

the isothermal compressibility diverges. It should be noted here that the cloud-point curve (or the coexistence curve) is the locus of pairs of η where the chemical potential and the pressure of the two coexisting phases became identical at a given τ and it is different from the points where the compressibility diverges, except at the critical point.

The coexistence curve which can be deduced from the use of Baxter's potential is highly skewed toward the low-volume-fraction side, a feature which is often experimentally observed in micellar solutions and microemulsions. This is due to the interaction which is short ranged and strong and is in sharp contrast to the wellknown van der Waals case, which is derived from an interaction that is long ranged and weak. To assess the degree of asymmetry on the gas and liquid sides, we have worked out the respective asymptotic behaviours

$$1 - \frac{\tau}{\tau_c} = 0.1584\left(1 - \frac{\eta}{\eta_c}\right)^2 \qquad \eta < \eta_c \tag{8}$$

$$1 - \frac{\tau}{\tau_c} = 0.0264\left(\frac{\eta}{\eta_c} - 1\right)^2 \qquad \eta > \eta_c. \tag{9}$$

The skewness can be assessed from the ratio of amplitudes in (8) and (9), namely 0.1584/0.0264=6. These equations also show that the PY approximation gives the mean-field exponent $\beta = \frac{1}{2}$. The mean-field theory is appropriate in a coarse analysis of the coexistence curve over a wide range of volume fractions. When making a fine analysis close to the critical volume fraction, the Ising value $\beta = 0.33$ has to be used and the mean field theory is not accurate.

One of the nicest feature of Baxter's model is, however, that one can also derive analytically the percolation loci in the (τ, η) plane. Coniglio *et al* [19] introduced a pair-connectedness function $P(r)$ in 1977, in connection with the development of a continuum

percolation theory. Given a particle at the origin, $4\pi r^2 \rho P(r)\, dr$ is the number of particles in the spherical shell $(r, r + dr)$ which are connected to this central particle and belong to the same cluster. Coniglio *et al* showed that $P(r)$ also satisfied an Ornstein–Zernike-type equation with a modified direct correlation function $c^+(r)$. By invoking the short-range nature of the direct correlation function, namely, $c^+(r) = 0$, for $r > a$, and the sticky-sphere condition

$$P(r) = \frac{\lambda a}{12}\,\delta(r - a) \tag{10}$$

Chiew and Glandt [20] were able to show that the average cluster size S is given by

$$S = \frac{1}{(1 - \lambda\eta)^2}. \tag{11}$$

The onset of percolation can be defined as the point where S diverges. Thus percolation loci in the (τ, η) plane are given by $\eta = 1/\lambda$, leading to an equation

$$\frac{1}{\tau} = \frac{12(1 - \eta)^2}{19\eta^2 - 2\eta + 1}. \tag{12}$$

Figure 5 shows also a percolation line according to (12).

In order to compare the theoretical phase diagram with the actual one, we have to specify the relationship between the stickiness parameter $1/\tau$ and the temperature. Equation (4) suggest that $1/\tau$ is proportional to the interaction strength and the effective interaction strength increases with temperature since there is a lower consolute point. The simplest relationship with two parameters α and γ is

$$\frac{\tau_c}{\tau} = 1 - \alpha\left(1 - \frac{T}{T_c}\right)^{\gamma}. \tag{13}$$

We can try to fit the experimental coexistence curve using the sticky-sphere model supplemented by (13) and then predict the percolation loci with it.

3. Analysis of SANS data below T_c

Extensive sets of SANS experiments have been performed in AOT/water/decane microemulsion systems as a function of temperature and volume fraction by replacing natural water by D_2O. As we said before this changes slightly the critical parameters and shift the phase diagram toward higher temperature by approximately 2 °C.

SANS intensity distribution from a system of polydispersed spherical droplets can be written as [21]

$$I(Q) = (\Delta\rho)^2 \varphi_W \left(\frac{4\pi}{3}\overline{R}^3\right) \frac{(Z + 6)(Z + 5)(Z + 4)}{(Z + 1)^3} \left|\overline{P}(Q)\right| \langle S(Q)\rangle \tag{14}$$

where $\Delta\rho = \rho_W - \rho_S$ is the difference of scattering-length densities of D_2O and protonated decane, ϕ_W the volume fraction of D_2O, $\overline{R} = \langle R\rangle$, the average radius of the water core, and Z the index related to the polydispersity (the width of the size distribution to the average

size of the droplets). The normalized, volume square averaged particle structure factor is defined as

$$\langle \overline{P}(Q) \rangle = \frac{1}{\langle R^6 \rangle} \left\langle R^6 \left(\frac{3j_1(QR)}{QR} \right)^2 \right\rangle. \tag{15}$$

The form factor of a spherical particle of radius R is $F(Q) = 3j_1(QR)/(QR)$, where $j_1(x)$ is the first-order spherical Bessel function. The form factor averaged interparticle structure factor for a system of p different sizes of droplet is defined as

$$\langle \overline{S}(Q) \rangle = \left\langle \sum_{ij}^{p} (\rho_i \rho_j)^{1/2} F_i(Q) F_j(Q) S_{ij}(Q) \right\rangle \Big/ \left\langle \sum_{i}^{p} \rho_i F_i^2(Q) \right\rangle. \tag{16}$$

The size average is taken with respect to a Schultz distribution, which is known to be accurate in the case of the AOT/water/decane system [2]. In this case the degree of polydispersity is $\Delta R/\langle R \rangle = (1 + Z)^{-1/2}$. The partial structure factor, $S_{ij}(Q)$, for a multicomponent sticky-sphere system has been given by Robertus *et al* [22], for $i, j = 1$–9, using Baxter's method. The FORTRAN package for calculating the partial structure factors has been kindly supplied to us by Dr J G H Joosten. The volume square averaged particle structure factor, assuming the Schultz distribution of sizes, had previously been given in an analytical form by Kotlarchyk and Chen [23]. Equation (14) contains three adjustable parameters $\langle R \rangle$, Z and τ enters in equation (14) through the Baxter's model expression for $S(Q)$. These parameters are functions of temperature and volume fraction. Here we assume that particles of different sizes have the same degree of stickiness.

Figure 6 shows results of fitting (14) to the intensity data from samples at $\phi = 0.08$, 0.10 and 0.12, all measured at $T = 40$ °C, closest to the critical temperature [24]. The three graphs on the left show experimental $I(Q)$, in log scale, against Q plots and their theoretical-analysis results (solid lines). The three graphs on the right depict the normalized, volume squared averaged particle structure factor and the form factor averaged interparticle structure factor extracted from the fits. The fits are satisfactory and from them we were able to extract, for all three samples, an averaged value of the water core $\langle R \rangle = (50 \pm 1)$ Å, close to what we estimated in section 1, and $Z = 8$, corresponding to a polydispersity index of 33%. The dimensionless stickiness parameter $\tau = 0.112$ for the 8% sample is the closest to the critical value $\tau_c = 0.0976$. From this we deduce that the critical volume fraction for the D_2O-based microemulsion system we studied is near 8%. This value is slightly different from that reported for the H_2O-based microemulsion system, namely 10%. As can be seen, the form factor averaged interparticle structure factor shows a zero-angle peak due to critical scattering and is devoid of the first diffraction peak due to low volume fractions. The slight wiggle around $Q = 0.2$ Å^{-1} is an artifact due to a finite sampling ($p = 9$) of the Schultz size-distribution function. It does not affect the quality of the fit because the average particle structure factor already decays to below 10^{-4} in this Q range.

Figure 7 shows results of the analyses of the temperature dependence of the scattering-intensity distributions for the 8% sample [24]. As temperature increases from 30 to 35 and to 40 °C the stickiness parameter progressively decreases toward the critical value, while the average size decreases and the width of the size distribution increases slightly.

4. Analysis of the phase diagram

What is most pleasing to see is, however, that the temperature variation of τ_c/τ derived from SANS data comes out in the form given in (13). This situation is similar to the case of

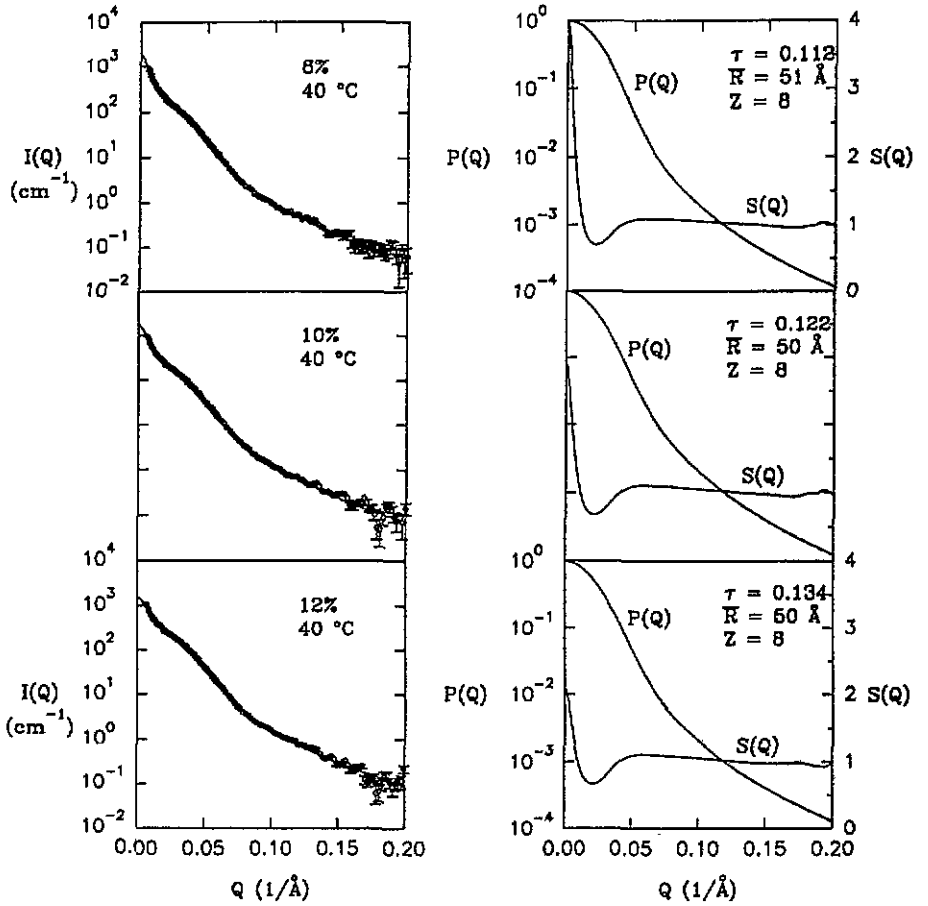

Figure 6. SANS intensity distributions and their analysis by Baxter's model with a polydispersity. *On the left of the figure, we show SANS intensity distributions for 8, 10 and 12% volume fraction* samples at 40 °C. The analysis shows that 8% case is closest to the critical volume fraction as indicated by the lowest value of τ obtained. In the right-hand part of the figure we present the corresponding particle structure factor $P(Q)$ and the interparticle structure factor $S(Q)$. It can be seen from the figure that $P(Q)$ for the three cases are almost identical indicating the same size and size distribution of the microemulsion droplets.

the non-ionic micellar solution investigated by Menon *et al* [25]. These authors suggested a linear relation between τ_c/τ and T/T_c. Figure 8 plots the τ_c/τ values obtained from analyses of SANS data against $(1 - T/T_c)^{0.94}$. Linear relations are obtained by adjusting the value of T_c. For the sample at a volume fraction of 8%, the fitted value of T_c turns out to be 42.7 °C, close to the actual T_c in a D_2O-based microemulsion system. The slope of the straight line gives $\alpha = 11.03$ in (13).

We shall derive (13) heuristically in the following way. We study the low-Q behaviour of the form factor averaged structure factor $S(Q)$ for a system of sticky hard spheres of an average diameter 100 Å and a polydispersity index $Z = 10$ at the critical volume fraction $\eta_c = 0.1213$. Figure 9 shows that at sufficiently small Q, the Ornstein–Zernike functional form is obtained and we can thus extract the long-range correlation length ξ as a function of τ as we approach the critical point. Figure 10 shows log–log plots of the correlation

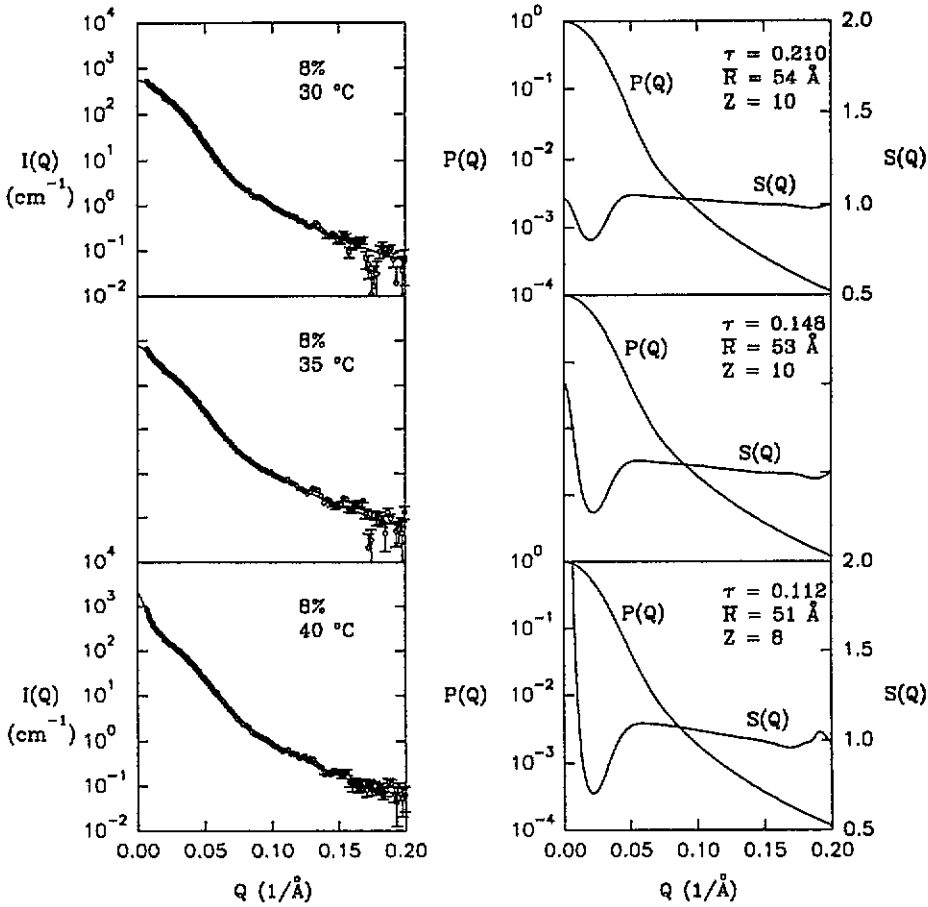

Figure 7. SANS intensity distributions of the 8% sample as function of temperature. It is notable that $S(Q)$ increasingly peaks in the forward direction as the temperature approaches the critical point. But the particle sizes and size distributions stay the same.

length ξ against $(1 - \tau_c/\tau)$. We obtain a series of straight lines implying the validity of a relation

$$\xi \approx \left(1 - \frac{\tau_c}{\tau}\right)^{-\nu'} \tag{17}$$

where the exponent ν' depends on the polydispersity index Z. When Z is very large, namely, when the system is monodisperse sticky spheres, $\nu' = 0.5$; but when $Z = 10$, corresponding to the system under study, $\nu' = 0.532$. On the other hand, it is known experimentally as well as theoretically that near the critical point of a fluid, the correlation length is a function of the temperature distance from the critical point according to

$$\xi \approx \left(1 - \frac{T_c}{T}\right)^{-\nu} \tag{18}$$

with $\nu = 0.5$, as in a mean-field theory like the PY approximation. Equations (17) and (18) taken together lead to our previous *ansatz* (13) in which $\gamma = \nu/\nu' = 0.500/0.532 = 0.94$.

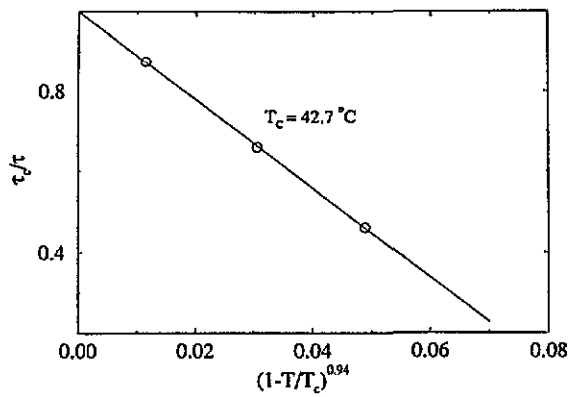

Figure 8. The inverse of the stickiness parameter τ extracted from SANS data for 8% volume fraction is plotted as a function of $(1-T/T_c)^{0.94}$ in order to obtain the slope $\alpha = -11.03$ and T_c. This value of α is used to calculate the theoretical coexistence curve. It is remarkable that the T_c obtained from the 8% data agrees with the experimental T_c measured for AOT microemulsions made with D_2O.

Figure 11 shows a comparison of the experimental cloud-point curve (stars) and the theoretical coexistence curve (solid line) and spinodal line (short-dashed line) calculated by taking monodisperse sticky spheres (using the average size of the polydisperse real system as the size of the monodisperse theoretical model) with the stickiness parameter $1/\tau$ depending on temperature according to the relation

$$\frac{\tau_c}{\tau} = 1 - 11\left(1 - \frac{T}{T_c}\right)^{0.94}. \tag{19}$$

In order to account completely for the percolation loci using (12) and (13), we have to introduce a temperature-dependent effective sticky-sphere diameter. This idea is a reasonable one because the definition of connectivity of two spheres should be dependent on the way it is measured experimentally, and so depends on the thermodynamic state of the liquid. In fact it is intuitively appealing to postulate that the higher the temperature the easier it is for the counterions to migrate from one water core of a droplet to another in the neighbourhood. Therefore the effective diameter of the microemulsion droplets, as far as the electrical percolation is concerned, is larger for higher temperatures. Figure 11 shows the result of force fitting the experimental percolation loci (diamonds) with (12) (long-dashed line) for volume fractions up to 0.4. Indeed, for larger values of the volume fraction the theoretical percolation line (12) differs significantly from the percolation line of the Baxter's model, as shown via computer simulations in [17]. The ratio $(\eta_{SHS}/\eta)^{1/3}$, which is a measure of the ratio of the effective diameter to the actual diameter, turns out to be a linear function of T/T_c. It is shown in figure 12 as a solid line.

5. Dynamics of the droplet-number density fluctuations near the critical point

We shall turn next to the discussion of some aspects of the droplet dynamics near the critical point. The study of the structure and dynamics of complex systems in term of clusters has been undertaken in many fields from nucleation theory [26], where cluster formation and

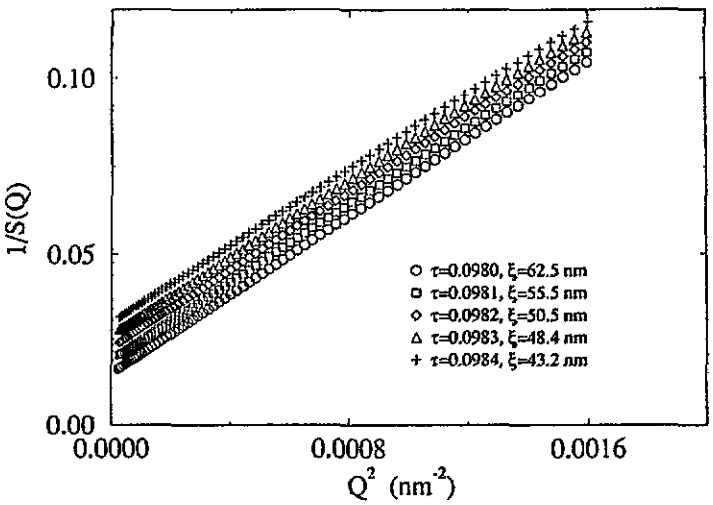

Figure 9. Small-Q behaviour of the $S(Q)$ function near the critical point for a volume fraction 0.1213 with $Z = 10$ and $a = 100$ Å. The graph shows that $S(Q)$ follows the Ornstein–Zernike function at sufficiently small Q so that the correlation length ξ can be extracted. It can be seen that as τ approaches τ_c ($= 0.0976$) the correlation length increases.

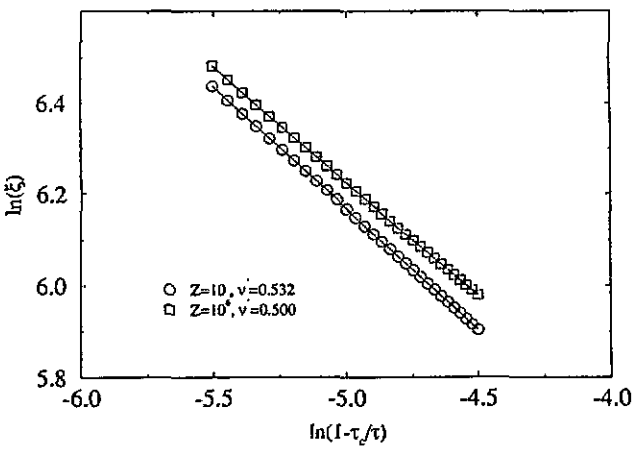

Figure 10. The dependence of the extracted correlation length on $(1 - \tau_c/\tau)$. It is seen that near the critical point, this is a power-law dependence with an index ν. For a monodisperse system (corresponding to large Z), ν' is 0.5. As the polydispersity increases (corresponding to decreasing values of Z), the value of ν' increases. At 33% polydispersity, ν' is 0.532.

growth lead to the formation of a stable phase from an unstable supercritical solution, to critical phenomena in which the cluster structure and dynamics is supposed to control the behaviour of the system close to criticality [27, 28], as well as in transport phenomena in disordered materials [14, 29]. We are here interested in the possibility of interpreting scattering data in terms of independent clusters, close to the critical point. In more precise words, we require a procedure to partition the N monomers in a system in N_c clusters containing N_n particles each, in such a way that

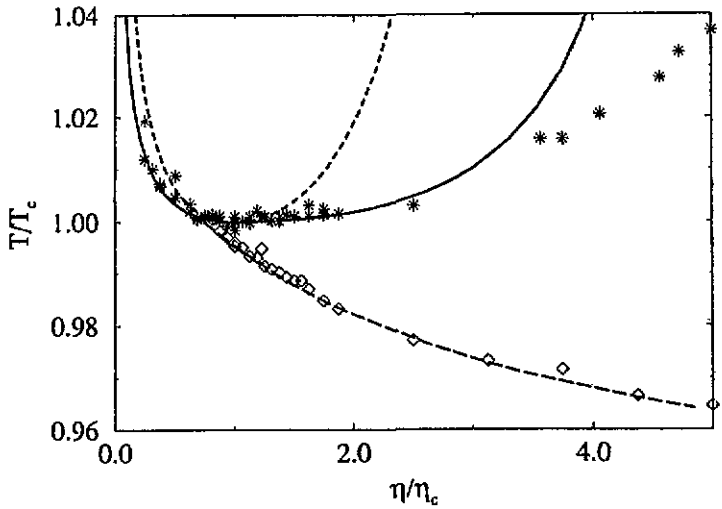

Figure 11. Experimental cloud points and the corresponding theoretical coexistence and spinodal curves based on Baxter's model after the transformation of (13), with $\alpha = 11$ and $\gamma = 0.94$ (see text). The percolation loci were fitted with Baxter's model using the method described in next figure caption.

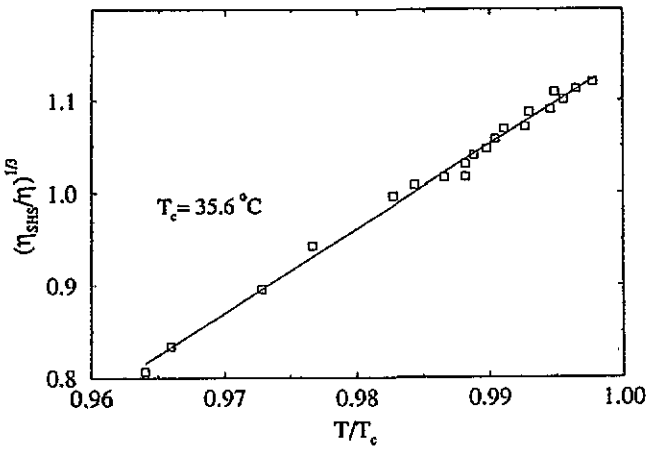

Figure 12. The temperature dependence of the apparent volume fraction η_{SHS} of sticky spheres which are needed to fit the percolation line. We plot the ratio $(\eta_{SHS}/\eta)^{1/3}$ versus T/T_c which results in a straight line. This shows that the apparent diameter of sticky spheres which are percolating increases as the temperature increases.

$$S(Q) = \frac{1}{N}\left\langle\left|\sum_{i=1}^{N} e^{iQ\cdot r_i}\right|^2\right\rangle = \frac{1}{N}\left\langle\left|\sum_{n=1}^{N_c}\sum_{i=1}^{N_n} e^{iQ\cdot(R_n+u_{ni})}\right|^2\right\rangle \tag{20}$$

becomes equal to

$$S(Q) = \frac{1}{N}\left\langle\sum_{n=1}^{N_c}\left|\sum_{i=1}^{N_n} e^{iQ\cdot u_{ni}}\right|^2\right\rangle \tag{21}$$

where R_n and u_{ni} are respectively the position of the centre of mass and the relative displacement of monomer i in the nth cluster. The equality between the two expressions underlines the requirement that clusters behave as independent units, i.e. with no correlation among them. Describing the system as a collection of N_c independent clusters allows us to write static and dynamic scattering properties in a straightforward way.

It has been recognized for a long time that the simple definition of clusters in terms of groups of closely interacting monomers does not produce independent clusters [30]. Only recently have Coniglio and Klein [31] been able to show in a formal way, for the Ising model, that independent clusters can be generated by breaking clusters of nearby parallel spins into smaller ones. According to Coniglio and Klein, nearby parallel spins are said to belong to the same cluster only with a probability $1 - e^{-2\beta J}$, where J is the interaction energy. Clusters so defined have the remarkable property of percolating at the critical point and being characterized by the same thermal critical exponents. In other words, the equality between (20) and (21) above holds not only at the critical point but all along the critical isochore, and not only at $Q = 0$ but for all wavevectors. We show this effect in figure 13, where the structure factor, evaluated from a two-dimensional 128×128 Monte Carlo simulation of an Ising model at three selected temperatures, is reported for both (20) and (21) using Coniglio and Klein's procedure. The intensity scattered by the collection of clusters is coincident with the intensity scattered by the whole system, considered as made up of individual interacting spins. The Lorentzian line shape of scattered light can thus be written as a sum of the scattering of polydisperse fractal clusters, characterized by a polydispersity index τ and a fractal dimension D. The exponents τ and D are related to the thermal critical exponents for the coexistence curve β and correlation length ν by $D = d - \beta/\nu$ and $D(\tau - 1) = d$. The independent-cluster picture can be generalized to the off-critical case if the asymmetry in the concentration of up and down spins is properly taken into account [32].

The starting point of our theory is an assumption that the slow dynamics of the droplet density fluctuation is dominated by diffusive motions of the independent percolation clusters [33]. This assumption is expected to be good in the vicinity of the percolation threshold, where large fractal clusters are formed. Formation of the fractal clusters is a necessary condition for the dynamic percolation theory [12, 13] to be valid. We have used it to explain the conductivity exponent below the percolation threshold in section 1. In the AOT/water/decane system, as one can see from the phase diagram (figure 1), the critical point is only about 2 °C above the percolation point. One therefore expects that the cluster structure and cluster size distribution in the critical region are similar to those at the percolation point.

For light scattering, the wavelength of visible light is much larger than the droplet sizes. Hence, for this Q range, the particle structure factor is nearly unity and we can ignore it. In order to deduce the dynamic structure factor $S(Q, t)$ of a collection of independent clusters, we first calculate the interparticle structure factor $S_k(Q)$ for a cluster containing k particles and having a radius of gyration R_k. We do this by Fourier transforming the cluster pair-correlation function [23]

$$\rho\left[g_k(r) - 1\right] = \frac{D}{4\pi R_1^D} \frac{1}{r^{3-D}} \exp\left(-\frac{r}{R_k}\right). \tag{22}$$

From this, Chen and Teixeira [34] deduced the static structure factor of a fractal aggregate. Their result, valid for small scattering wave number Q, relevant for light scattering, can be

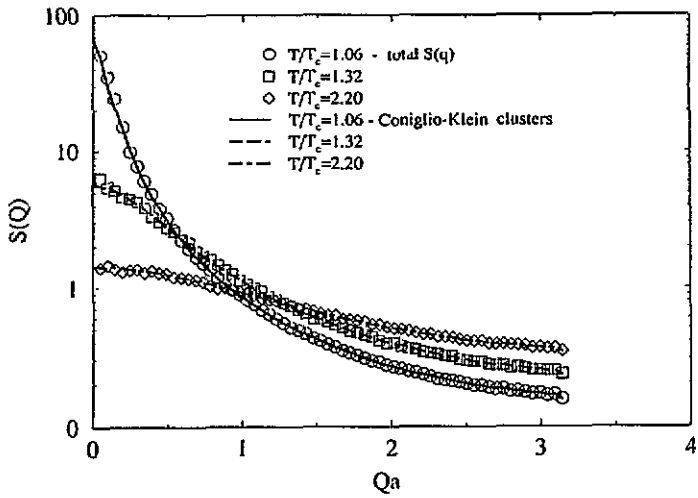

Figure 13. Structure factor $S(q)$ evaluated from a two-dimensional 128 × 128 Monte Carlo simulation of an Ising model at three selected temperatures. The structure factor has been evaluated according to (20) and (21) of the text, assuming that monomers are sitting in all up-spin sites. Symbols are $S(q)$ evaluated according to (20). Lines are $S(q)$ evaluated according to (21), defining clusters according to the Coniglio–Klein prescription. This result shows that it is possible to find a prescription to divide the spins into clusters such that the scattered intensity can be written either summing over the individual spins or summing over the independent clusters.

written as

$$S_k(Q) = k\frac{\sin\left[(D-1)\,\tan^{-1}(QR_k)\right]}{(D-1)\,QR_k\left(1+Q^2R_k^2\right)^{(D-1/2)}}. \tag{23}$$

The radius of gyration R_k of the k cluster is connected to the radius R_1 of a single droplet by

$$R_k = R_1 k^{1/D}. \tag{24}$$

From (23) one can derive [33] the following approximate expression for the static structure factor of a k cluster valid at low Q values:

$$S_k(Q) \approx k\exp\left(-\tfrac{1}{3}Q^2R_k^2\right). \tag{25}$$

This approximation seems to be an essential one in the theory because it leads to a nice analytical form for the average relaxation rate which reduces to a well known Kawasaki formula in the limit of small droplet size to be discussed next.

We use the following expression for the normalized cluster size distribution function $N(k)$, proposed by Stauffer [35] for random percolation, and recently confirmed for the independent clusters close to the critical point by Wang [32].

$$kN(k) = \frac{S^{\tau-2}}{\Gamma\left(2-\tau, 1/S\right)}\,k^{1-\tau}\exp\left(-\frac{k}{S}\right) \tag{26}$$

where $\Gamma(x, y)$ is the incomplete Euler gamma function and S, the cut-off of the cluster size distribution, is proportional to $\langle k \rangle^{1/(3-\tau)}$. The normalized dynamical structure factor is then given in this model by

$$S(Q,t) = \left(\int_1^\infty \mathrm{d}k \; kN(k)S_k(Q) \; \exp\left(-D_k Q^2 t\right) \right) \left(\int_1^\infty \mathrm{d}k \; kN(k)S_k(Q) \right)^{-1} \tag{27}$$

where D_k, the diffusion coefficient of the k cluster, is given by

$$D_k = D_1 k^{-1/D}. \tag{28}$$

D_1 is the renormalized diffusion coefficient of a single droplet. It is written in the form

$$D_1 = R \frac{k_B T}{6\pi \mu R_1} \tag{29}$$

where μ is the shear viscosity of the solution, and R is a fitting parameter which takes into account a possible deviation from the Stokes–Einstein law of diffusion.

The normalized scattered-intensity autocorrelation function $C(Q, t)$, a quantity which is experimentally measured in a dynamic light-scattering experiment, can be shown to be

$$C(Q,t) = 1 + |S(Q,t)|^2. \tag{30}$$

The average relaxation rate $\Gamma(Q)$ for the cluster diffusion is given by the first cumulant of $S(Q, t)$

$$\Gamma(Q) = -\lim_{t \to 0} \left[\frac{\mathrm{d}}{\mathrm{d}t} \ln (S(Q,t)) \right]. \tag{31}$$

To put the relaxation rate $\Gamma(Q)$ into a universal form depending only on a scaling parameter x, we first define the correlation length $\xi = \left(R_1/\sqrt{3}\right) S^{1/D}$ and then the scaling variable by $x = Q\xi$. The other non-dimensional parameter representing the lower limit of the cluster sizes is defined by $x_1 = \left(1/\sqrt{3}\right) Q R_1$. From the above definitions, one can express the reduced first cumulant $\Gamma^*(x, x_1)$ in terms of the two non-dimensional parameters by

$$\Gamma^*(x, x_1) = \frac{\Gamma(Q)}{D_1 R_1 Q^3}. \tag{32}$$

The reduced first cumulant is explicitly given by

$$\Gamma^*(x, x_1) = \frac{3\pi}{8} \frac{\Gamma\left(3 - \tau, x_1^D\right)}{\Gamma\left(3 - \tau - 1/D, x_1^D\right)} \frac{\Gamma(3 - \tau - 1/D, u)}{\Gamma(3 - \tau, u)} \left(1 + \frac{1}{x^2}\right)^{1/2} \tag{33}$$

where $u = (x_1/x)^D (1 + x^2)^{D/2}$. Note that the reduced first cumulant Γ^* explicitly depends on the reduced size x_1 of the monomer. Thus the average relaxation rate of the order parameter relevant to the critical phenomenon cannot be written just as a product of a universal function of the scaling variable $x = Q\xi$ and a system-dependent function, as is in the case for the mode-coupling or mode-decoupling theories of critical dynamics in simple liquids.

In order to compare in more details the predictions of this model with the classical theory of critical phenomena, one has to evaluate both the fractal dimension and the polydispersity index for the critical clusters. As far as percolation is concerned, numerical simulations [35] gave universal values for the indices $D = 2.5$ and $\tau = 2.2$. These indices are connected by a hyperscaling relation [35] involving the space dimension d

$$\tau = \frac{d + D}{D} \tag{34}$$

which implies $\tau = 2.2$ when taking $D = 2.5$, in agreement with the simulation result. As we mentioned before, the concentration fluctuation of the particle system can be represented by a cluster diffusion of independent clusters having a fractal dimension D given by

$$D = d - \frac{\beta}{\nu} \tag{35}$$

where $\beta = 0.33$ and $\nu = 0.63$ are respectively the Ising universal exponents of the coexistence curve and of the long-range correlation length, and $d = 3$ is the dimensionality of space. From (35) we infer $D = 2.5$ which, when introduced into the hyperscaling relation, (34) leads to $\tau = 2.2$. These two values are equal to the fractal dimension and the polydispersity index of percolating clusters.

To get more accurate estimates of D and τ, we can use a set of scaling laws known in the theory of critical phenomena to eliminate the factor β/ν on the right-hand side of (35). In fact we know that in $d = 3$, $\beta/\nu = (1 + \eta)/2$, so that

$$D = \frac{5 - \eta}{2} \tag{36}$$

and the polydispersity index τ is then given by the hyperscaling relation as

$$\tau = \frac{11 - \eta}{5 - \eta}. \tag{37}$$

Taking the accepted value of the Fisher exponent $\eta = 0.03$, we obtain $D = 2.49$ and $\tau = 2.21$. These values of the indices will be used as input parameters when fitting experiments to theory.

Very close to the critical point where ξ is much larger than R_1, the reduced first cumulant becomes a universal function of $x = Q\xi$. It reduces exactly to the Perl and Ferrel [36] mode-decoupling result when $R_1 = 0$, and in this case it is also numerically very close to the Kawasaki formula [37]

$$\lim_{x_1 \to 0} \Gamma^*(x, x_1) = \frac{K(x)}{x^3} \tag{38}$$

where $K(x)$ is the Kawasaki dynamic scaling function

$$K(x) = \frac{3}{4}\left[1 + x^2 + \left(x^3 - \frac{1}{x}\right) \tan^{-1}(x)\right] \tag{39}$$

which is known to account very well for light-scattering data near critical points of one-component fluids or binary mixtures of molecular liquids. $\Gamma^*(x, x_1 = 0)$ has the simple asymptotic behaviour

$$\Gamma^*(x, x_1 = 0) = \frac{a}{x} \qquad x \ll 1 \tag{40}$$

$$\Gamma^*(x, x_1 = 0) = b \qquad x \gg 1 \tag{41}$$

where a and b are known constants. Figure 14 illustrates the crossover from small-x to large-x behaviour as expressed in (40) and (41). Using light-scattering data taken near the critical point of the AOT/water/decane system, we illustrate the agreement of measured first cumulants of photon correlation functions and the prediction of (33). It is clear from the graph that the finite-size effect of microemulsion droplets is large enough to be detectable in a light-scattering experiment.

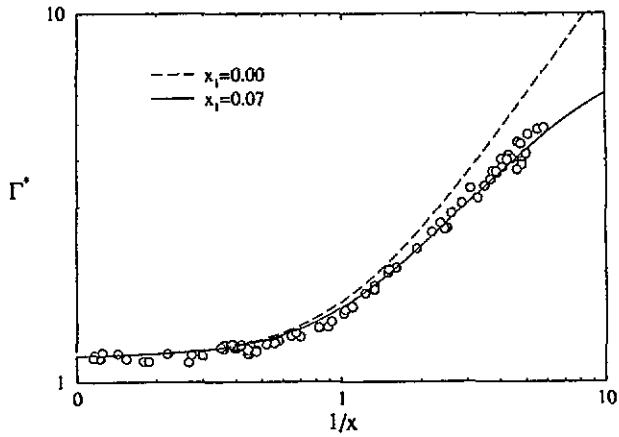

Figure 14. The dynamic scaling function $\Gamma^*(x, x_1)$ associated with the average relaxation time of the cluster diffusion plotted as a function of $1/x$ for two values of the scaled droplet size x_1. Open circles are experimental data from the AOT/water/decane system near the critical point. The broken line corresponds to Kawasaki's mode–mode-coupling result. The solid line is the result of the improved version of the dynamic droplet model presented in the text.

From (27) we can further derive the time dependence of the photon correlation function $S(u, v)$

$$S(u, v) = \frac{1}{\Gamma(3 - \tau, u)} \int_0^\infty \mathrm{d}z\, z^{2-\tau} \exp\left(-z - vz^{-1/D}\right) \tag{42}$$

in terms of the dimensionless variable u previously defined and an additional dimensionless time variable $v = D_1 R_1 Q^3 t(1 + x^{-2})^{1/2}$. It is sufficient for our purpose here to state that at sufficiently short time $\Gamma t \ll 1$, (42) can be analytically integrated and leads to an exponential decay for the photon correlation function

$$S(u, v \to 0) = 1 + \exp[-2\Gamma(Q)t] \tag{43}$$

where Γ is the first cumulant already defined in (31). At long time ($\Gamma t \gg 1$), the integral can also be evaluated analytically by using the steepest-descent method. In this regime, the photon correlation function asymptotically approaches a stretched exponential form

$$S(u, v \gg 1) = 1 + \exp\left[-2(\overline{\Gamma}t)^\beta\right] \tag{44}$$

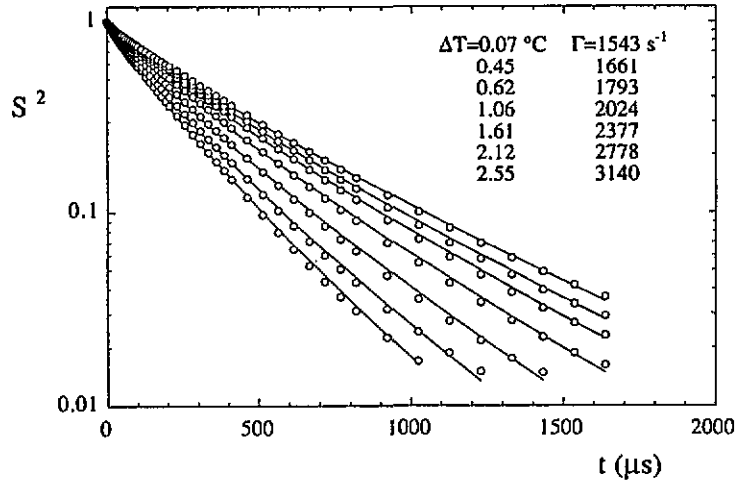

Figure 15. Experimental correlation functions taken from the AOT/H_2O/decane system near the critical point using a logarithmic photon correlator. Note the non-exponential behaviour at long time.

where the exponent $\beta = D/(D+1)$ is the universal number 0.713 and $\overline{\Gamma}$ is given by

$$\overline{\Gamma} = \beta^{1/\beta} D^{1/D} D_1 R_1 Q^3 \left(1 + \frac{1}{x^2}\right)^{1/2}. \tag{45}$$

The crossover from the short-time exponential decay to the long-time stretched exponential decay of the photon correlation function occurs at the dimensionless variable $\Gamma t = 1$. Figure 15 gives several photon correlation functions measured near the critical point. From these semilogarithmic plots, one can see the extent of the deviation from exponentiality at long time. At the critical volume fraction, i.e. for a dilute sample, deviations from the exponential decay never amount to more than a few per cent. These small deviations can be detected experimentally only by the use of a logarithmic photon correlator having a very stable base line [38]. One has to stress at this point that one expects to observe the purely stretched exponential decay only for very large values of Γt, say $\Gamma t \gg 10^2$, a region which presently cannot be accessed experimentally. Therefore a deduction of the fractal dimension from the fitting of photon correlation function to a stretched exponential form in the practical domain of measurements would produce an incorrect result. In particular, since the experimental data are usually taken in the crossover regime, such a fitting procedure would give a value of fractal dimension smaller than the universal one. As a final comment we want to point out that the independent-clusters model is an evolution of the dynamic droplet model introduced by Martin and Ackerson [28]. The differences consist in the explicit consideration of the existence of a lower cut-off length scale given by the finite size of the monomers, which is not always negligible compared to the correlation length. The situation is different in the case of molecular liquids, where the lower cut-off length is always small compared to the correlation length. The existence of a finite lower cut-off length in micellar solutions and microemulsions introduces a non-universal characterization of the system. Another important difference from Martin and Ackerson is in the choice of the exponents τ and D that characterize the independent clusters and their distribution. For the calculation of scattering properties one must select truly independent clusters.

6. Dynamics of the droplet-number-density fluctuations near the percolation threshold at high volume fractions

As we stated above, the phase behaviour and concentration fluctuations of dilute microemulsions having volume fractions lower than 40% and above 30 °C are dominated by the existence of the critical point. However the percolation phenomenon and the associated cluster formation is the dominant factor controlling the dynamics of microemulsions at higher volume fractions and lower temperatures. One of the most significant findings of this research is the realization that the droplet dynamics near the percolation threshold is in many way similar to that near the critical point because both phenomena are controlled by cluster dynamics. The quantitative difference between the two lies in the magnitudes of the average cluster sizes at some given distances from the critical and percolation points where measurements are made.

In the percolation regime the Gaussian approximation of (25) for the k-cluster static structure factor is no longer sufficient and a more complicated form, taking into account the fractal scattering, is necessary [33]. From this consideration, it can be shown that the reduced first cumulant of the dynamic structure factor, defined in the same way as in section 5, can be written as

$$\Gamma^*(x) = \frac{F(3-\tau-1/D,x)}{G(x)}\left(1+\frac{1}{x^2}\right)^{-(D/2)(3-\tau-1/D)} + \left(1+\frac{1}{2\rho^2}\right)\frac{H(2-\tau-1/D,x)}{G(x)}\left(\frac{x}{h}\right)^{-D} \tag{46}$$

where ρ is the ratio of the hydrodynamic radius the radius of gyration of the clusters. The functions $F(a,x)$, $H(a,x)$ and $G(x)$ are defined in the following way:

$$F(a,x) = \Gamma(a) - \Gamma\left(a, \left(h^2\frac{1+x^2}{x^2}\right)^{D/2}\right) \tag{47}$$

$$H(a,x) = \frac{\sin[(D-1)\pi/2]}{D-1}\Gamma\left(a, \left(\frac{x}{h}\right)^{-D}\right) \tag{48}$$

$$G(x) = F(3-\tau,x)\left(1+x^2\right)^{-(D/2)(3-\tau)} + H(2-\tau,x)\left(\frac{x}{h}\right)^{-D} \tag{49}$$

and the scale variable x is related to the average cluster size by

$$x = hQR_1S^{1/D} \tag{50}$$

where $h = \sqrt{D(D+1)/6}$. The reduced average relaxation rate (first cumulant) shows the asymptotic behaviour $\Gamma^*(x) = 1/x$ when $x \ll 1$ and constant when $x \gg 1$. In figure 16 the reduced average relaxation rate deduced from dynamic light scattering experiments has been plotted as a function of $1/x$ for different temperatures and volume fractions. This graph includes our experimental data [39] and some other data taken from measurements performed by Chen and Huang [40], Sheu *et al* [21] and Magazù *et al* [41]. These data

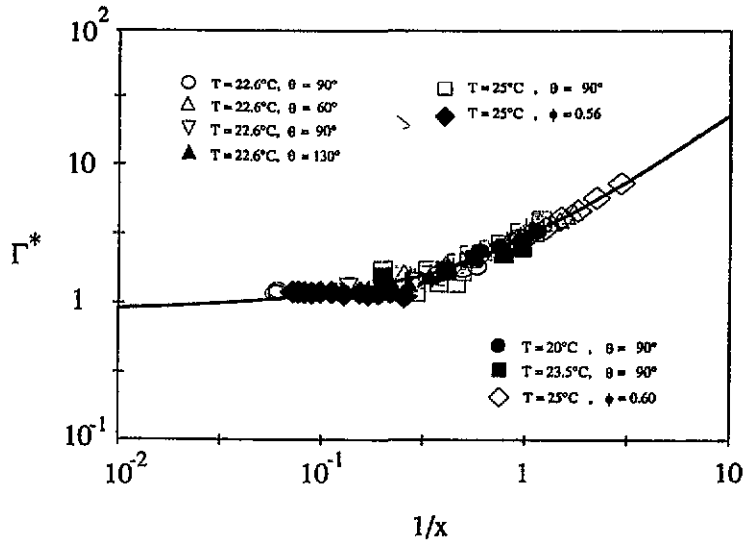

Figure 16. Scaling plot of the scaled first cumulant as a function of the scaled variable $1/x$ close to percolation.

span a rather large domain of x i.e. $0.1 \leqslant x \leqslant 10$ and allow us to study the crossover regime from the classical hydrodynamic Q^2 behaviour to the percolation Q^3 behaviour. This feature is very well accounted for by our model.

Along the same lines as developed above, we have also been able to derive the time evolution of the dynamic structure factor and from that calculate the photon correlation function. A rather complicated expression has been obtained [33]. The important point is that near the percolation threshold one can also observe two different regimes: at low value of the reduced time $\Gamma t \ll 1$, the formula predicts an exponential decay whereas for a large value of the reduced time, it predicts a stretched exponential decay, characterized by a universal exponent identical to the one for the critical phenomena, namely, $\beta = 0.713$. These predictions have been verified experimentally. In figure 17 are depicted photon correlation functions taken at a constant temperature but for different values of volume fraction. A very good agreement can be observed between our experimental results and the model in a wide range of volume fractions. A numerical calculation of the photon correlation function has also been performed over a large domain of the reduced time in order that $S(Q, t)$ can be fitted to a stretched exponential function. This domain corresponds to Γt from zero to 100. An interesting crossover phenomenon is predicted by the calculation: a strong deviation from the single-exponential decay should occur at a value of Γt close to unity. This prediction has been verified experimentally (figure 18). At high volume fractions, it is very easy to detect experimentally the deviation from the initial exponential decay, in contrast to the situation near the critical point where the deviations are very small. This is due to the fact that near the critical point the average cluster size is of the order of 1000 while near the percolation point it is of the order of 50 000. Thus the diffusion of an average percolation cluster is roughly five times slower than that of the average critical cluster. This brings the time window for which the crossover to the stretched exponential is predicted into an experimentally accessible range of the photon correlation function for the case near the percolation point.

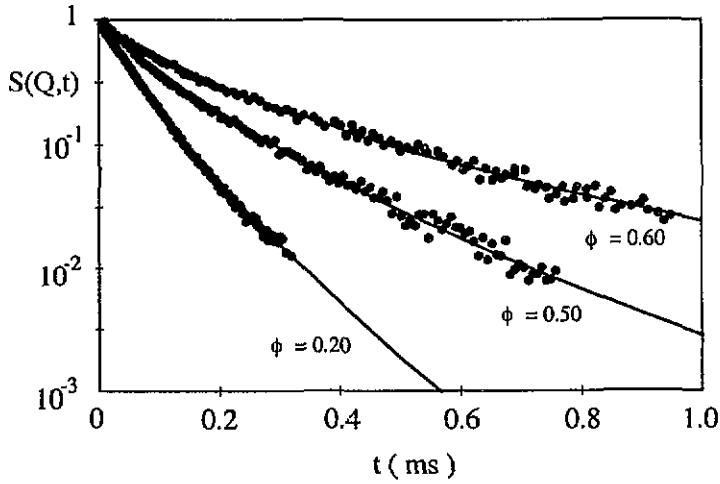

Figure 17. Time correlation function for various volume fractions close to percolation, from [40], taken at $T = 22.6$ °C and a 90° scattering angle. The solid lines are given by the theory described in the text, with $\beta = 0.713$.

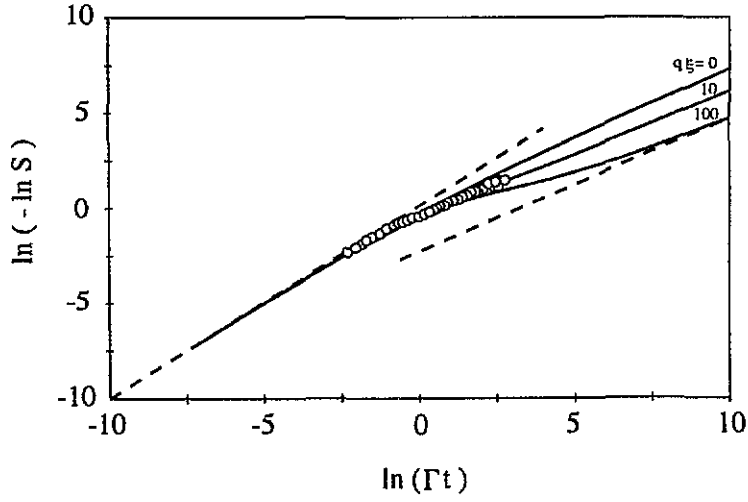

Figure 18. Double logarithmic plot of the dynamic structure factor for various values of the adimensional variable Γt. The dashed lines indicate the limiting slopes corresponding to an exponential and a stretched exponential.

7. *Dielectric relaxation*

We turn now to dielectric-relaxation measurements close to the percolation threshold. We measured in a wide frequency range, from 100 kHz to 1 GHz, and in a large concentration domain, from 0.2 to 0.64 in volume fraction of the dispersed phase, the conductivity and the dielectric constant of the microemulsion [43]. The data are shown in figure 19. The low-frequency behaviour has been analysed in terms of power-law behaviours both below and above percolation, with the critical exponents s' and t typical of dynamic and static percolation we mentioned at the beginning. At percolation the intermediate-frequency

behaviour, for both σ and ϵ, is characterized by a power law ω^u with the exponent $u = t/(s' + t)$. The physical mechanism for the sudden increase in conductivity on approaching the percolation threshold has been interpreted in term of formation of transient clusters of microemulsion droplets. Such clusters offer a path for the motion of charge carriers among different droplets. The finite conductivity below percolation is related to the continuous restructuring of the clusters, with a typical time T_r, allowing the carriers to move across the sample even if at any time no infinite cluster exists. This description of the conductivity below the percolation threshold, named dynamical or stirred percolation [12, 13], is able to explain the value of the critical exponent as $s' = 2\beta - \nu$, where β is the exponent related to the probability of belonging to the infinite cluster and ν is the exponent for the divergence of the connectivity length. s' is different from the exponent s describing the divergence of conductivity below T_p in a static conductor–superconductor mixture. A complementary physical description which is able to explain the presence of finite conductivity below percolation is obtained by considering a simple mixture of materials of different conductivity. In such a case, the ratio of the conductivities plays a role similar to the restructuring time in the dynamical percolation model. The exponents s and s' are obtained by different assumptions on the scaling behaviour of the number of boundary sites between the two materials. A nice feature of these models is that they can be extended into the high-frequency domain. In a dynamical percolation model, the presence of a finite restructuring time introduces a crossover between the high-frequency $\omega \ll 1/T_r$ regime, where the behaviour is similar to the static percolation and the low-frequency regime, in which the rearrangement time plays a significant role. In the static mixture model, the frequency behaviour can be studied by introducing reactive elements. In the simple resistance–capacitance mixture, which in our case could be identified with the oil (mostly capacitive) and with the disperse phase (mostly resistive), the value of the resistance multiplied by the capacitance fixes the crossover frequency. Both models imply that the relaxation phenomena for the complex conductivity $\Sigma = \sigma + i\omega\epsilon$, which gives with its real part the conductivity and with its imaginary part the permittivity multiplied by the frequency, obey a scaling relation given by the scaling function Φ

$$\Sigma = \Delta p^t \ \Phi(c\,\Delta p^{-(s'+t)}) \tag{51}$$

in terms of the scaling variable $x = c\,\Delta p^{-(s'+t)}$, where c is the ratio of the complex conductivities and Δp is the parameter which measures the distance from percolation [14] in composition or in temperature. The scaling function Φ below percolation can be developed in a series starting as $\Phi(x) \approx x$ and evolves into an asymptotic behaviour for large x values as $\Phi(x) \approx x^u$.

This type of scaling has been derived in the case of model binary systems on a lattice, in two-component electric circuits [14] and in the study of diffusion on clusters [12, 44, 45]. The latter approach is the most interesting one since it describes the conductivity as a sum of contributions of independent clusters. Indeed the average mean square displacement is written as a sum of the squared displacements of the diffusing walkers over the clusters composing the system. The structure of the underlying fractal cluster is reflected in the value of the mean square displacement and allows a connection of the diffusivity anomaly indices with the percolation indices. To clarify the connection with the cluster picture, we write the conductivity as [12, 44]

$$\sigma \approx \int_1^\infty \mathrm{d}k\ N(k)\frac{r_k^2(T_r)}{T_r} \tag{52}$$

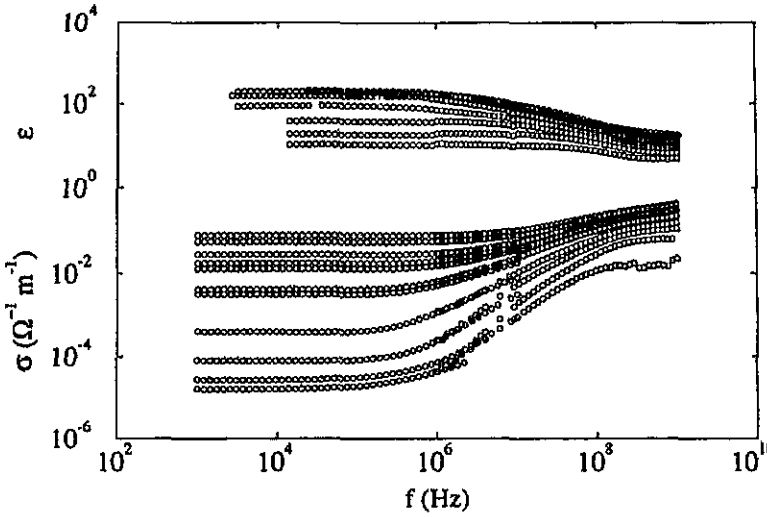

Figure 19. The measured conductivity σ and the relative dielectric constant ϵ as a function of frequency for the following volume fractions: 0.20, 0.24, 0.28, 0.32, 0.36, 0.40, 0.44, 0.48, 0.52, 0.56, 0.60, 0.64, from bottom to top for both quantities

where $r_k^2(T_r)$ is the squared displacement of a walker on a k cluster during the typical cluster rearrangement time T_r. The corresponding diffusivity $r_k^2(T_r)/T_r$ can then be expressed as $(R_k^2/T_r)f(\tau_k/T_r)$, where f is a scaling function of the ratio of the time τ_k it takes the charge carrier to visit all the sites in a typical k cluster to the cluster rearranging time. The outcomes of such an approach are a good description of both the static and relaxational properties of conductivity and dielectric constant at percolation. In fact with a proper choice of the scaling function $f(\tau_k/T_r)$ [46] it is possible to describe many aspects of the relaxation process, including the presence of a finite static conductivity below and at the threshold when the conductivity of the solvent is different from zero. It is also possible to explain the power-law behaviour of the complex conductivity at percolation and the value of the corresponding exponent u (figure 20).

8. Conclusions

We have given concrete evidence that both the structure and dynamics observed in a three-component microemulsion system, AOT/H_2O or D_2O/decane, near the critical point can be explained in terms of a model based on the formation of transient, polydisperse fractal clusters due to a short-range attraction between microemulsion droplets. This attractive interaction increases in a specific way as the temperature increases toward the critical point. We derive a quantitative relation between the interaction strength and the temperature from analyses of SANS data in the one-phase region approaching the critical point. This relation is used to explain the overall features of the phase diagram, including the cloud-point curve and the percolation line. The diffusive cluster dynamics also accounts for the temperature and the Q dependence of the first cumulant of photon correlation functions in the critical region. The dynamic scaling function associated with the average relaxation rate deviates significantly from the well known Kawasaki function away from the critical point due to the large sizes of the microemulsion droplets [38]. In this respect the so-called dynamic

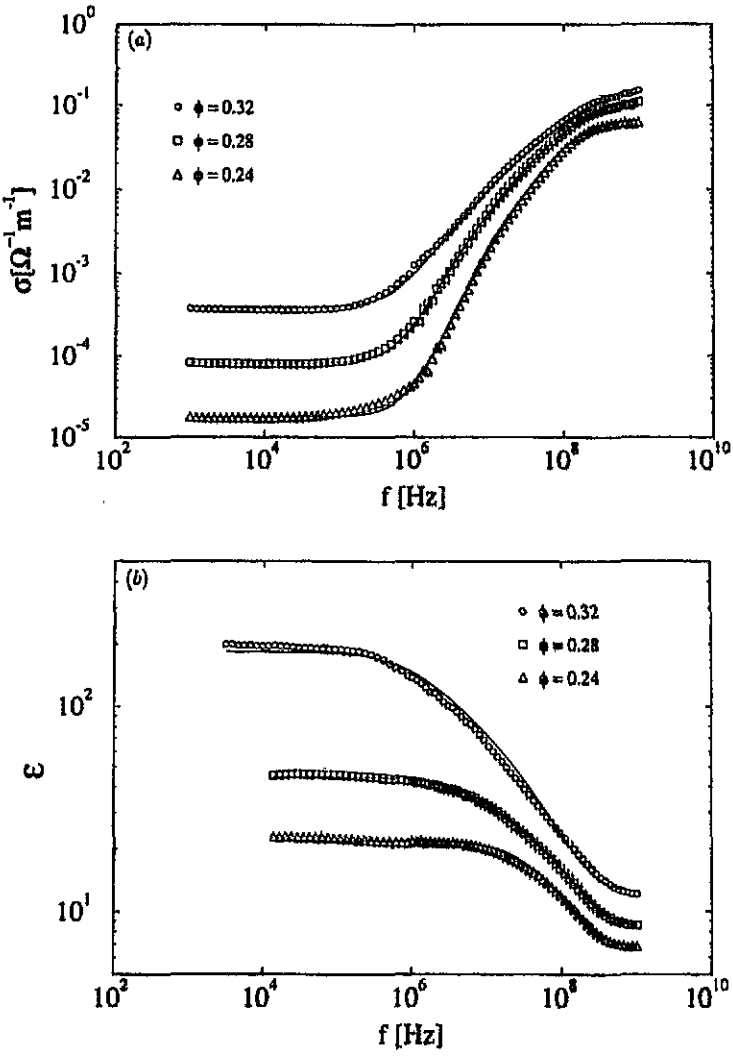

Figure 20. (*a*) Scaling plot of the scaled first cumulant as a function of the scaled variable $1/x$ close to percolation [46]. (*b*) Relative dielectric constant as a function of the frequency for the same samples as in (*a*).

background effects are taken into account in a very natural way by this improved version of the dynamical droplet model. The size of the microemulsion droplet turns out to be an important parameter of the theory. The long-time behaviour of the photon correlation function $S(Q, t)$ is shown to be asymptotically a stretched exponential form with a universal stretch exponent of 0.713 [33]. Experimental measurements of $S(Q, t)$, approaching the critical point, can be made only in the crossover regime for practical reasons. They show, however, small but significant deviations from exponential decay at long time, in full agreement with the theory. The dynamic slowing down of the relaxation rate can also be readily observed by dynamic light scattering approaching and near the percolation loci at higher volume fractions [21, 33, 40]. The first cumulant of photon correlation functions near and approaching the percolation line shows a slowing down and a Q-crossover phenomenon

much the same as that near the critical point. The only difference between the two lies in the dependence of the average cluster size on the distance to the percolation or the critical point [42]. Dielectric-relaxation measurements close to the percolation threshold can also be interpreted in terms of formation of transient clusters of microemulsion droplets, which offer a path for the motion of charge carriers. Experimental data satisfy scaling relations not only statically, as a function of composition and temperature, but also as a function of frequency between 100 kHz and 1 GHz. Again it is possible to describe the experimental data below and at percolation in terms of sums over clusters of different size relaxing with different times. The amplitude and relaxation time of the clusters are written in terms of scaling quantities as a function of their size.

Acknowledgments

The research of S H Chen is supported by a grant from the Materials Science Division of the U S Department of Energy. The research of F Sciortino and P Tartaglia is supported by GNSM/CNR and Consorzio INFM/MURST. We are grateful to C Y Ku for supplying many figures presented in this article. Part of this work was done in collaboration with Professor C Cametti and Dr P Codastefano. J Rouch would like to acknowledge a NATO collaboration grant for travel support to the USA.

References

[1] Kahlweit M, Strey R, Firman P, Hasse D, Jen J and Schomcker R 1988 *Langmuir* **4** 499
Kalweit M, Strey R, Schomcker R and Hasse D 1988 *Langmuir* 5 305
Kahlweit M 1992 *Structure and Dynamics of Strongly Interacting Colloids and Supramolecular Aggregates in Solution (NATO ASI Series C369)* ed S H Chen, J S Huang and P Tartaglia (Dordrecht: Kluwer) p 231
[2] De Geyer A and Tabony J 1986 *Chem. Phys. Lett.* **124** 357
[3] Scriven L E 1976 *Nature* **263** 123
[4] Chen S H, Chang S L and Strey R 1990 *J. Chem. Phys.* **93** 1907
[5] Kotlarchyk M, Chen S H, Huang J S and Kim M W 1984 *Phys. Rev. Lett.* **53** 914
[6] Kotlarchyk M, Chen S H, Huang J S and Kim M W 1984 *Phys. Rev.* A **29** 2054
[7] Auvray L, Cotton J P, Ober R and Taupin C 1984 *J. Phys. Chem.* **88** 4586
[8] Lichterfeld F, Schumeling T and Strey R 1986 *J. Phys. Chem.* **90** 5762
[9] Chen S H, Chang S L, Strey R, Samseth J and Mortensen K 1991 *J. Phys. Chem.* **95** 7427
[10] Rouch J, Safouane A, Tartaglia P and Chen S H 1989 *J. Chem. Phys.* **90** 3756
[11] Cametti C, Codastefano P, Tartaglia P, Rouch J and Chen S H 1990 *Phys. Rev. Lett.* **64** 1461
[12] Grest G S, Webman I, Safran S and Bug A L R 1986 *Phys. Rev.* A **33** 2842
[13] Lagues M 1979 *J. Physique Lett.* **40** L331
[14] Clerc P, Giraud G, Laugier J M and Luck J M 1990 *Adv. Phys.* **39** 191
[15] Menon S V G, Manohar C and Srinivasa Rao K 1991 *J. Chem. Phys.* **95** 9186
[16] Baxter R J 1968 *J Chem. Phys.* **49** 2770
[17] Kranendonk W G and Frenkel D 1988 *Mol. Phys.* **64** 403
[18] Barboy B 1974 *J. Chem. Phys.* **61** 3194
[19] Coniglio A, De Angelis U and Forlani A 1977 *J. Phys. A: Math. Gen.* **10** 1123
[20] Chiew Y C and Glandt E D 1983 *J. Phys. A: Math. Gen* **16** 2599
[21] Sheu E Y, Chen S H, Huang J S and Sung Y C 1989 *Phys. Rev.* A **39** 5867
[22] Robertus C, Philipse W H, Joosten J G H and Levine Y K 1989 *J. Chem. Phys.* **90** 4482
[23] Kotlarchyk M and Chen S H 1983 *J. Chem. Phys.* **79** 2461
[24] Chen S H, Ku C Y, Rouch J and Tartaglia P 1994 *12th Symp. on Thermo-physical Properties (Boulder, CO, 1994)*
[25] Menon S V G, Kelker V K and Manohar C 1990 *Phys. Rev.* A **43** 1130
[26] Abraham F F 1974 *Homogeneous Nucleation Theory* (New York: Academic)

[27] Fisher M E 1967 *Physics* **3** 255
[28] Martin J E and Ackerson B J 1985 *Phys. Rev.* A **31** 1180
[29] Stauffer D and Aharony A 1992 *Introduction to Percolation Theory* (London: Taylor and Francis)
[30] Muller Krumbhaar H 1979 *Monte Carlo Methods in Statistical Physics* ed K Binder (Heidelberg: Springer)
[31] Coniglio A and Klein W 1980 *J. Phys. A: Math. Gen.* **13** 2775
[32] Wang J S 1989 *Physica* A **161** 249
[33] Tartaglia P, Rouch J and Chen S H 1992 *Phys. Rev.* A **45** 7257
[34] Chen S H and Teixeira J 1986 *Phys. Rev. Lett.* **57** 2583
[35] Stauffer D 1979 *Phys. Rep.* **54** 1
[36] Perl R and Ferrell R A 1972 *Phys. Rev. Lett.* **29** 51; *Phys. Rev.* A **6** 2358
[37] Kawasaki K 1976 *Phase Transitions and Critical Phenomena* vol 5A, ed C Domb and M S Green (New York: Academic) p 165
[38] Rouch J, Tartaglia P and Chen S H 1993 *Phys. Rev. Lett.* **71** 1947
[39] Chen S H, Rouch J and Tartaglia P 1992 *Croatica Chem. Acta* **65** 353
[40] Chen S H and Huang J S 1985 *Phys. Rev. Lett.* **55** 1888
[41] Magazù S, Majolino D, Maisano G, Mallamace F and Micali N 1989 *Phys. Rev.* A **40** 2643
[42] Chen S H, Mallamace F, Rouch J and Tartaglia P 1992 *Slow Dynamics in Condensed Matter* ed K Kawasaki, T Kawakatsu and M Tokuyama (New York: American Institute of Physics) p 301
[43] Cametti C, Codastefano P, Di Biasio A, Tartaglia P and Chen S H 1989 *Phys. Rev.* A **40** 1962
[44] Gefen Y, Aharony A and Alexander S 1982 *Phys. Rev. Lett.* **50** 77
[45] Hong D C, Stanley H E, Coniglio A and Bunde A 1986 *Phys. Rev.* B **33** 4564
[46] Cametti C, Chen S H, Rouch J, Sciortino F and Tartaglia P to be published